Journal of Nuclear Materials 395 (2009) 69–74

Contents lists available at ScienceDirect

Journal of Nuclear Materials

journal homepage: www.elsevier.com/locate/jnucmat

# Zirconolite-rich titanate ceramics for immobilisation of actinides – Waste form/HIP can interactions and chemical durability

Y. Zhang *, M.W.A. Stewart, H. Li, M.L. Carter, E.R. Vance, S. Moricca

*Institute of Materials Engineering, Australian Nuclear Science and Technology Organisation, PMB 1, Menai, NSW 2234, Australia*

ARTICLE INFO

*Article history:*
Received 12 June 2009
Accepted 29 September 2009

ABSTRACT

Zirconolite-based titanate ceramics containing U plus Th or Pu have been prepared. The final consolidation to produce a dense monolithic waste form was carried out using hot isostatic pressing (HIPing) of the calcined materials within a stainless steel can. The ceramics were characterised and tested for their overall feasibility to immobilise impure Pu or separated actinide-rich radioactive wastes. As designed, tetravalent U and Pu are mainly incorporated in a durable zirconolite phase, together with Gd or Hf added as neutron absorbers. The interaction of the waste form with the HIP can was also examined. No changes in the U valences or the U/Pu-bearing phase distributions were observed at the waste form–HIP can interface.



## 1. Introduction

Synroc-C, an assemblage of geological stable titanate minerals, plus minor amounts to encapsulated alloys, was first developed in the 1970s for immobilisation of high-level nuclear waste (HLW) derived from Purex-type reprocessing of spent nuclear fuels [1,2]. The waste form mineral phase assemblage was designed to incorporate the radioisotopes via substitution for elements in the target mineral crystal lattices. For example: actinides (Ac) and rare earth (RE) fission products were targeted to enter zirconolite ($CaZrTi_2O_7$) via, e.g., $Pu^{4+} \Leftrightarrow Zr^{4+}$ and $2(RE,Ac)^{3+} \Leftrightarrow Ca^{2+} + Zr^{4+}$; $Sr^{2+}$ for $Ca^{2+}$ in perovskite ($CaTiO_3$); and, $Cs^+$ or $Rb^+$ ions in the $Ba^{2+}$ site of hollandite [$Ba(Al,Ti)_2Ti_6O_{16}$]. Some fission products such as Mo, Tc, Ru, Rh, and Pd formed very fine metallic particles encapsulated within the waste form ceramic matrix. Since then, various synroc derivatives have been developed and extensively studied [2–8], both in the laboratory and via natural analogue minerals, as potential candidates for immobilisation of a range of diverse high-level radioactive waste streams. Zirconolite, one of the key mineral components for many synroc formulations, has long been recognised as a radiation resistant [9,10] and chemically durable [11,12] phase, suitable to host actinides. In the mid-1990s, zirconolite-rich and pyrochlore-rich formulations were developed for immobilisation of surplus plutonium [13,14]. In these formulations Gd and Hf were added as neutron absorbers to address the criticality issue during processing, interim storage and long-term disposal of the final waste forms.

Zirconolite, as a derivative of the fluorite structure type, can be viewed as a condensed version of the pyrochlore structure [15]. It consists of alternating layers of (Ca, Zr) polyhedra and Ti polyhedra. The main differences between the pyrochlore ($A_2B_2X_6Y$) and zirconolite structures are that pyrochlore contains three dimensional arrays of corner-linked B–X octahedra whereas zirconolite contains only two dimensional Ti–O octahedra, and that A cations in pyrochlore are strongly bonded to only two anions, whilst in zirconolite Ca-, Zr- and Ti-site cations are 8-, 7- and 6-fold coordinated, respectively [5]. The end-member of titanate-based zirconolite is $CaZrTi_2O_7$ (2*M* polytype), in which Ca and Zr have 8- and 7-fold coordination, respectively, with no site symmetry elements other than the identity operator [5]. Different polytypes (e.g. 3*T*, 3*O*, 4*M*) arise through solid solutions towards lanthanide and actinide-bearing end-members [4].

Uranium can be incorporated into both the Ca and Zr sites of zirconolite as tetravalent ions [16]. Pentavalent uranium can also be formed in samples sintered in an oxidative environment [16,17]. Like U, Pu can also be incorporated into the Ca and Zr sites in zirconolite [3]. The presence of $Pu^{4+}$ in zirconolite has been determined by XANES (X-ray absorption near-edge spectroscopy) and DRS (diffuse reflectance spectroscopy) in air-fired samples [18–20] whilst up to 80% of Pu ions can be reduced to the trivalent form when the sample is sintered in a reducing atmosphere [19]. In addition, it has been demonstrated using Pu-doped perovskites that Pu valences, either tetravalent or trivalent, have very little effect on the overall chemical durability of the titanate materials [21].

Hot isostatic pressing (HIPing) was first developed in the US in the 1950s [22] and today is widely applied in the heat treatment of both ceramics and metal alloys [23]. Components to be processed are placed in an electrically heated furnace, inside a pressure vessel, and pressure applied by compressing a gas, such as argon. Under high temperature and pressure, the components bond together

* Corresponding author. Tel.: +61 2 9717 9156; fax: +61 2 9543 7179.
*E-mail address:* Yingjie.Zhang@ansto.gov.au (Y. Zhang).

0022-3115/$ - see front matter 
doi:10.1016/j.jnucmat.2009.09.019

physically, sinter and/or react chemically to form a dense solid material. For densification of porous or powdered materials, the samples to be HIPed are placed into a container, typically metal or glass, which is then evacuated and hermetically sealed. The HIPing route has been shown to be particularly useful for processing of high-level radioactive wastes as it offers some advantages over the conventional methods (such as sintering or melting). As the consolidation of the waste form takes place within an enclosed can [24,25], there are no high temperature volatility losses and hence less of a need for large, expensive off-gas systems. HIPing also provides a flexible process platform able to handle multiple waste streams [26]. Furthermore, unlike baseline borosilicate glass technologies, the HIP process is not dependant upon the properties of a melt (such as viscosity, electrical conductivity and crystal formation). As a result, waste loadings can be higher and the HIP process can handle problematic wastes not suitable for borosilicate glasses and can be made with higher waste loadings. This results in substantial life-cycle waste disposition savings [27]. In addition, secondary wastes, such as used melters, are eliminated, further decreasing life-cycle costs.

During HIP processing, the waste form and the container, typically stainless steel [24–27], used for containment of the waste form may interact with each other. Previously we have reported such interactions for an inactive synroc sample containing mainly zirconolite, hollandite and rutile [24]. The main interactions at the interface are localised oxidation of the stainless steel can and reduction of the ceramic. As the main feature for such interactions, oxidised Fe and Cr diffuse and transfer from the stainless steel can to the synroc phases. However, possible ceramic/can interactions on the actinide-bearing phase distribution near the interface need to be verified for real plutonium-bearing materials.

In the current work, zirconolite-based formulations were chosen to confirm their overall feasibilities for immobilisation of impure Pu wastes or separated minor actinides through the HIP processing technique, including characterisations of actinide-bearing phases, actinide valences, waste form/HIP-can interactions under HIP conditions, and chemical durability of the waste forms.

## 2. Experimental

The U/Th-doped sample formulation was nominally 90% zirconolite (containing Gd) and 10% Ba-hollandite. The Pu-doped sample was nominally 80% of zirconolite (containing Gd and Hf), plus ~10% each of Ba-hollandite and rutile [14]. Both formulations were designed to incorporate Pu and neutron absorbers into the zirconolite phase (with Pu on the Ca site, Hf on the Zr site and Gd equally distributed on the Ca and Zr sites). The hollandite was present in the formulations to provide a host phase for radioactive Cs. This would provide the option of using an internal radiation barrier to prevent or reduce the threat of theft of Pu during the formation and transport of the waste form [13,14].

The oxide compositions for both U/Th-doped and Pu-doped samples are given in Table 1. The U/Th-doped sample (200 g) was prepared by the oxide route [28], calcined in air at 700 °C for 2 h, 2 wt.% Ni was added and the powder placed inside a HIP can, which was then evacuated and sealed. This was then hot isostatically pressed (HIPed) at 1280 °C and 100 MPa for 3 h under an argon atmosphere. The HIP can was made from 2 mm thick 316 stainless steel. The Pu-doped sample (20 g) was prepared in the similar way as the U/Th-doped sample and was HIPed using a 4 mm thick 304 stainless steel can at 1280 °C under an argon atmosphere.

Polished samples were prepared for electron microscopy characterisation of phases formed in the bulk materials. The interface samples were cut for characterisation of the interactions between stainless steel and the waste form. The samples were cross sectionally mounted in epoxy resin, and polished to a 0.25 mm diamond finish.

**Table 1**
Calculated oxide compositions (wt.%) of the two zirconolite-rich samples.

| Oxide | U/Th-doped sample | Pu-doped sample |
|---|---|---|
| $Al_2O_3$ | 4.20 | 6.86 |
| BaO | 2.25 | 2.26 |
| CaO | 9.37 | 5.93 |
| $TiO_2$ | 42.50 | 40.12 |
| $ZrO_2$ | 24.69 | 13.03 |
| $Gd_2O_3$ | 8.07 | 8.69 |
| $HfO_2$ | – | 10.10 |
| $ThO_2$ | 4.41 | – |
| $UO_2$ | 4.51 | – |
| $PuO_2$ | – | 13.00 |

Round disc specimens, 8 mm in diameter and 2 mm thick, for durability testing were taken from the bulk materials and polished to a 0.25 mm diamond finish on their large faces. The durability tests were carried out at 90 °C in duplicate in deionised water, according to the ASTM leaching protocol [29]. The test was modified in that leachates were completely replaced with fresh leachant after 1 and 7 days, with a total leaching time of 28 days for the U/Th doped specimens; leachate replacement was carried out after 7 and 35 days, with a total leaching time of 84 days for the Pu-doped specimens. The same surface area to volume ratio (SA/V = 0.1 $cm^{-1}$) was used for all the tests. Pu contents in the leachates were analysed by using alpha-spectrometry whilst the other elements were analysed by using ICP-MS (Inductively Coupled Plasma – Mass Spectrometry).

Scanning electron microscopy (SEM) on polished surfaces of samples was carried out on a JEOL 6400 instrument run at 15 kV and fitted with a Tracor Northern TN5502 energy-dispersive spectrometer (EDS). Diffuse reflectance spectra were collected at ambient temperature using a Cary 500 spectrophotometer equipped with a Labsphere Biconical Accessory. Spectra are referenced to that of a Labsphere certified standard (Spectralon), and transformed into Kubelka–Munk units, $F(R) = (1 - R)^2/2R$ [30].

## 3. Results and discussion

### 3.1. Characterisation by electron microscopy of the bulk waste forms

#### 3.1.1. U/Th-doped sample

A SEM backscattered electron image of the bulk material (Fig. 1) showed two main phases, zirconolite (~89 vol.%) and hollandite (~8 vol.%), with trace amounts of brannerite (~2 vol.%), and metallic Ni (<1 wt.%, <75 μm) added as powder to control redox during HIPing. No perovskite was observed, which is not unexpected as reducing conditions sufficient to reduce some $Ti^{4+}$ ions to $Ti^{3+}$ are required to form perovskite in zirconolite ceramics [31].

The oxide compositions of zirconolite, hollandite and brannerite (nominally $UTi_2O_6$) are shown in Table 2, although the exact composition of the brannerite was difficult to determine due to the very small grain size; however it is known that $ThO_2$ promoted brannerite formation in pyrochlore-rich ceramics [28]. Note the presence of brannerite in a waste form has been shown to have little effect on the waste form overall chemical durability as brannerite is a relatively durable phase [28,32]. Uranium and thorium are overwhelmingly incorporated in the zirconolite and brannerite, together with the Gd.

#### 3.1.2. Pu-doped sample

The backscattered SEM electron image of the bulk material (see Fig. 2) indicated that the microstructure of the sample is similar to

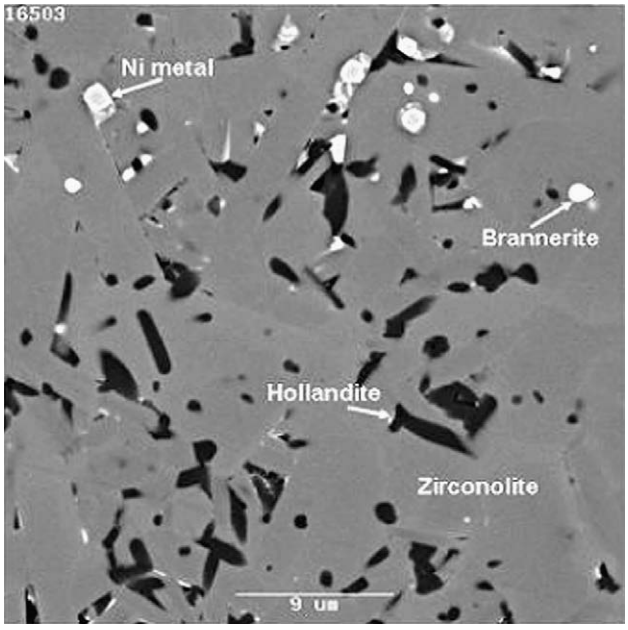


**Fig. 1.** SEM backscattered electron image of the polished U/Th-doped sample shows mainly zirconolite as the general matrix and hollandite with trace amounts of brannerite and metallic Ni particles.

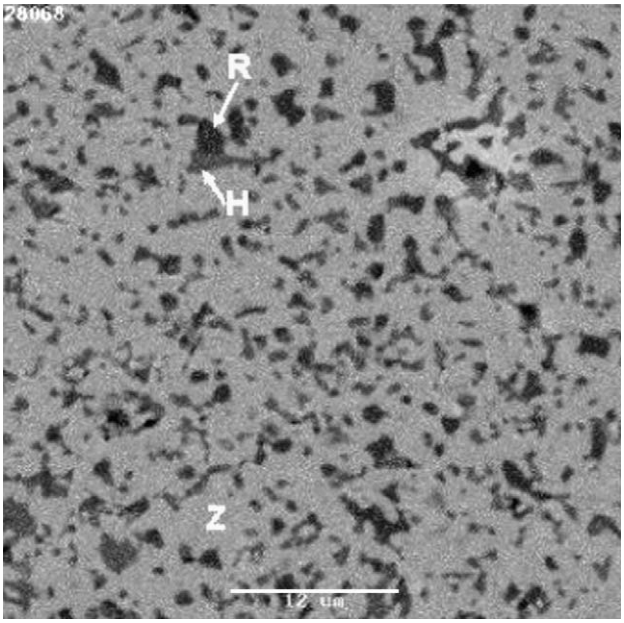


**Fig. 2.** SEM backscattered electron image of the polished Pu-doped sample shows primarily zirconolite (light matrix-Z), hollandite (H) and rutile (R).

**Table 2**
Main oxide composition of zirconolite, hollandite and brannerite in the U/Th-doped sample.

| Oxide | Zirconolite (wt.%) | Hollandite (wt.%) | Brannerite (wt.%) |
|---|---|---|---|
| $Al_2O_3$ | 3.3 | 7.7 | – |
| BaO | – | 26.9 | – |
| CaO | 10.7 | – | – |
| $Gd_2O_3$ | 9.2 | – | 1.7 |
| $ThO_2$ | 4.4 | – | 34.0 |
| $TiO_2$ | 39.9 | 65.4 | 39.2 |
| $UO_2$ | 4.4 | – | 19.7 |
| $ZrO_2$ | 28.0 | – | 4.9 |

the U/Th-doped sample. The Pu-doped sample contained mainly zirconolite (~90%) and hollandite (~8%), together with small amounts of Hf-bearing rutile (~2%). As designed, the Pu was completely incorporated in zirconolite phase together with Gd and Hf as neutron absorbers. Again, no perovskite was observed in the microstructure. Brannerite was also not observed. This is primarily believed to be due to the smaller ionic radius of $Pu^{4+}$ ions compared to $Th^{4+}$ and $U^{4+}$ ions, and $Pu^{4+}$ lies at the lower A site size ionic limit of stability for brannerite ($A_2Ti_2O_6$) [32]. It is apparent that the target phase assemblage has been closely achieved.

### 3.2. Waste form/HIP-can interactions under HIPing conditions

#### 3.2.1. U/Th-doped sample

Waste form/HIP-can interactions of an inactive synroc sample have been studied previously [24]. The interface interactions were dominated by Fe and Cr diffusion from stainless steel into synroc. In the current work, the U/Th-doped sample has been used to verify the previous finding and to examine if there is any effect of such interactions on the U-bearing phase distribution near the interface. A SEM backscattered electron image of the cross-sectional interface (Fig. 3) shows several numbered areas of interests. Some (Cr/Mn = 2:1)-rich oxide particles (**1**) ~2 μm in diameter, have been identified ~10 μm away from the interface on the stainless steel side. Small $SiO_2$ particles along the reaction interface on the stainless steel side have also been observed (**2**) and they are likely to be the result of oxidation and migration of trace amounts of Si in the 316 stainless steel (typical composition: Fe: 61.8–68.8%, C: 0.08%; Mn: 2.0%; P: 0.045%, S: 0.03%, Si: 1.0%, Cr: 16–18%, Ni: 10–14%, Mo: 2–3%) towards the reaction interface. Areas (**3**) and (**4**) are $(Cr, Fe, Al)_2O_3$ solid solutions containing trace amounts of $TiO_2$ (~1%), with higher Fe content in area **4** (~24%). Cr-rich hollandite (**5**), with nominal composition very close to ($Ba_{1.3}Al_{0.4}Fe_{0.1}Cr_{2.1}Ti_{5.4}O_{16}$), forms at the interface adjacent to the zirconolite front. Some small scattered Ni-rich metallic particles (**6**) are also present in areas **3** and **4**.

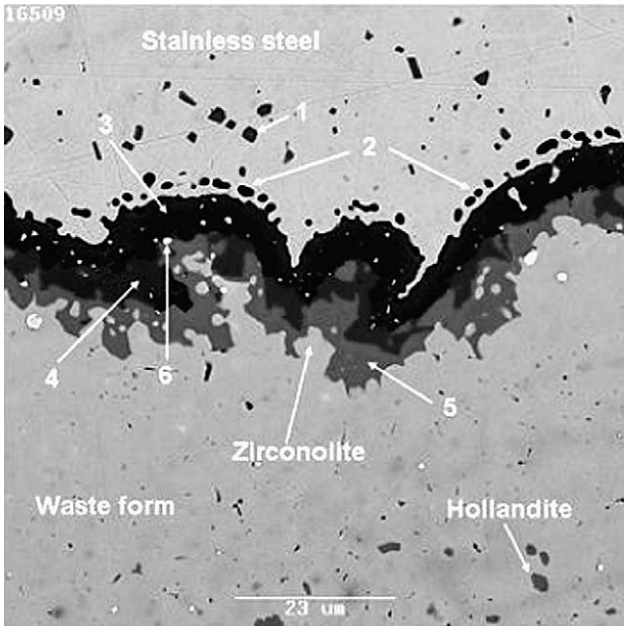


**Fig. 3.** SEM backscattered electron image of the cross-sectional interface for the U/Th-doped sample shows numbered areas of interest: (Cr/Mn = 2:1)-rich oxide particles (**1**); $SiO_2$ particles (**2**); $(Cr, Fe, Al)_2O_3$ solid solutions (**3** and **4**) with various amounts of Fe and Ti oxides; Cr-doped hollandite ($Ba_{1.3}Al_{0.4}Fe_{0.1}Cr_{2.1}Ti_{5.4}O_{16}$) (**5**) and Ni-rich metallic particle (**6**).

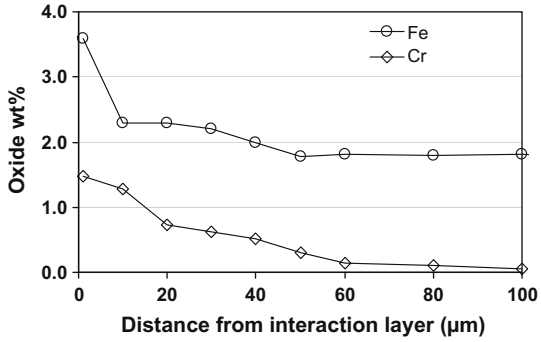


**Fig. 4.** Profiles of Fe and Cr oxide contents in zirconolite from interface towards the bulk.

The reaction zone of the waste form was observed to extend up to 50 μm from the can interface. The microstructure of this region is slightly different to the bulk material (Fig. 1), with less abundant hollandite. The profiles of Fe and Cr oxides in zirconolite from the reaction front towards the waste form, shown in Fig. 4, indicate that Cr and Fe diffuse into zirconolite about 100 μm and over 500 μm (100–500 μm not shown), respectively. The result is consistent with our previous work [23]. It has been shown that transition metals can be readily accommodated into the zirconolite lattice [33] and the zirconolite can self-charge compensate, e.g., $Gd^{3+}$ can reside on either the $Ca^{2+}$ or $Zr^{4+}$ site or cation vacancies can form.

The interfacial reaction–diffusion system here is relatively complex, being a multi-component, non-equilibrium system operating with redox changes in the ions present and requires further study, probably with simpler systems, to fully understand it. Despite the diffusion of Fe and Cr into the zirconolite matrix, the waste form/HIP-can interactions do not significantly change the U/Th-bearing phases at the reaction interface, with U/Th entirely incorporated in zirconolite and brannerite phases. Given that the purpose of the waste form is to immobilise actinides then one can conclude from this case that the HIP can has no effect upon this criterion.

### 3.2.2. Pu-doped sample

A SEM backscattered electron image of the cross-sectional interface of the Pu-doped sample is given in Fig. 5. The microstructure was observed to be somewhat similar to the interface in the U/Th-doped sample (Fig. 3) with small $SiO_2$ particles along the reaction interface on the stainless steel side (**1**), Cr-depleted stainless steel particles (**2**), grains of $(Cr_xAl_{1-x})_2O_3$ solid solution that contain variable amounts of Fe (7–17%) and Ti (3–11%) oxides (**3** and **4**), and Cr-rich hollandite (**5**) with the nominal composition similar to that found in the U/Th-doped sample.

The waste form HIP can reaction zone, up to 50 μm deep, has a slightly different microstructure to the bulk material (Fig. 2). The hollandite grains are larger than those in the bulk. However, as an interface reaction product, the Cr-rich hollandite (**5**) in both Pu and U/Th samples has slightly different appearance. In the case of U/Th-doped sample, it forms a continuous layer right at the reaction front on the waste form side. In contrast for the Pu-doped sample, it forms larger grains, compared to hollandite grains in the bulk waste form, evenly distributed up to 50 m in the reaction front of the waste form. The above difference is believed to be due to subtle diversity of local redox conditions. However, future work on Pu-doped samples may provide more evidence for better understanding of such phenomena.

As with the U/Th-doped sample, the waste form/HIP-can interactions for the Pu-doped sample do not seem to have any significant effect on the Pu-bearing phase distribution in the reaction zone with the Pu remaining wholly incorporated in zirconolite.

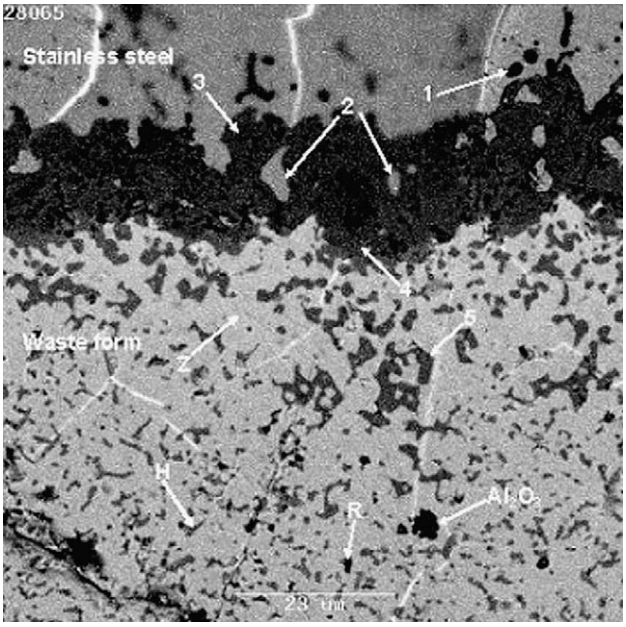


**Fig. 5.** SEM backscattered electron image of the cross-sectional interface for the Pu-doped sample shows labelled ceramic phases (Z – zirconolite, H – hollandite and R – rutile) and some numbered areas of interest: $SiO_2$ particles (**1**); Cr-depleted stainless steel particles (**2**); $(Cr_xAl_{1-x})_2O_3$ solid solutions (**3** and **4**) with various amounts of Fe and Ti oxides; and Cr-doped hollandite (**5**).

Nevertheless, the current work confirms that zirconolite-rich waste form/HIP-can interactions involve diffusion of Fe/Cr from stainless steel and Al/Ti from the waste form (at the expense of hollandite), forming mixed oxide solid solutions and Cr-rich hollandite at the interaction region.

### 3.3. Chemical durability of actinide-bearing zirconolite-rich waste forms

Leaching tests were carried out to verify the chemical durability of the waste forms produced. The normalised elemental release rates, based on geometrical surface areas, of the U/Th-doped sample in deionised water (DIW) are shown in Fig. 6. The dissolution of the waste form in DIW is incongruent with preferential releases of Al, Ba and Ca over Gd, Th, Ti, U and Zr. These results suggest that Gd, Th and U are incorporated in the more durable zirconolite phase as designed, consistent with the microscopic characterisations, with normalised elemental release rates all below $10^{-3}$ g m$^{-2}$ d$^{-1}$ after 28 days of leaching in deionised water.

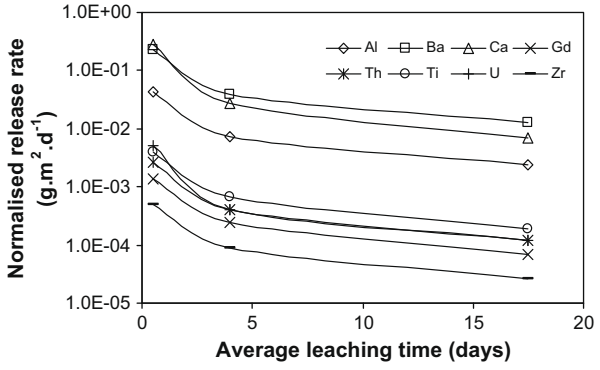


**Fig. 6.** Normalised elemental release rates (g m$^{-2}$ d$^{-1}$) of the U/Th sample leached at 90 °C in deionised water for 0–1, 1–7 and 7–28 days (midpoint of each leaching period is used).

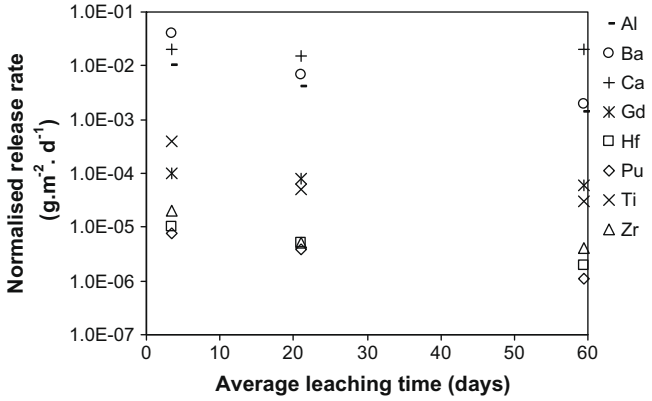


**Fig. 7.** Normalised elemental release rates ($g\,m^{-2}\,d^{-1}$) of the Pu-doped sample leached at 90 °C in deionised water for 0–7, 7–35 and 35–84 days (midpoint of each leaching period is used).

Similar to the observations for the U/Th-doped sample, the normalised elemental release rates of the Pu-doped sample in DIW show (see Fig. 7) preferential releases of Al, Ba and Ca over Gd, Ti, Pu, Hf and Zr, with normalised elemental release rates of Pu and Hf below $10^{-5}$ g m$^{-2}$ d$^{-1}$ after 35 days, and that of Gd between $\sim10^{-4}$ and $10^{-5}$ g m$^{-2}$ d$^{-1}$. The low and similar release rates of Pu and Hf and Gd from the waste form suggest that the neutron absorbers will remain in the ceramic with the Pu, unlike more mobile neutron absorbers, such as boron. In addition, if in the long run the Pu is released the Hf and to some extent the Gd will escort it. This will minimise the risk of criticality during waste form storage and in the long-term geological disposal [11]. These results are certainly in agreement with those of the early chemical durability testings for various synroc formulations [2,3].

Natural analogue studies [2,6–8] on U/Th zirconolites have revealed valuable information on radiation damage, long-term actinide retention and hydrothermal alterations of natural zirconolites. However, it is difficult to directly correlate the hydrothermal alterations to the laboratory leaching results for the synthetic zirconolites due to the unknown nature of the hydrothermal fluids present in a future repository. Nevertheless, the general loss of Ca, rare earths and slightly depleted U/Th in some of the alteration zones [6] are broadly consistent with the preferential release of Ca over U/Th identified in the above laboratory studies.

### 3.4. Actinide valences in zirconolite

#### 3.4.1. U in zirconolite

Both tetravalent and pentavalent uranium ions have been previously identified in zirconolite samples prepared at different redox conditions [16,17]. In principle, the f–f electronic transitions give numbers of sharp peaks with half width of a few hundred cm$^{-1}$ in the near infrared. The absorption spectrum of $U^{5+}$ ($f^1$ configuration) ion in zirconolite consists of a sharp band at 6650 cm$^{-1}$, and three broader bands at 9270, 10,720 and 13,400 cm$^{-1}$, due to spin–orbit coupling and crystal field splitting in an octahedral environment [17]. In contrast to $U^{5+}$, a large number of components (90) arise from the splitting of the states of the $f^2$ configuration of $U^{4+}$, under spin–orbit coupling and crystal field effects. DR spectra of the U/Th-doped sample and a single-phase U-doped zirconolite ($CaZr_{0.8}U_{0.2}Ti_2O_7$) sample, in the near infrared range, are shown in Fig. 8. Clearly both spectra exhibit no features of $U^{5+}$ ions and they have been assigned to the spectra of $U^{4+}$ ions in zirconolite [16]. As the zirconolite phase near the reaction interface is exposed to a more reducing environment due to the presence of the stainless steel HIP-can, uranium should continue to favour the state of tetravalent as $U^{3+}$ will not form in oxide systems [34]. The waste form/HIP-can interactions therefore, should have no detectable effect on uranium valences near the reaction interface.

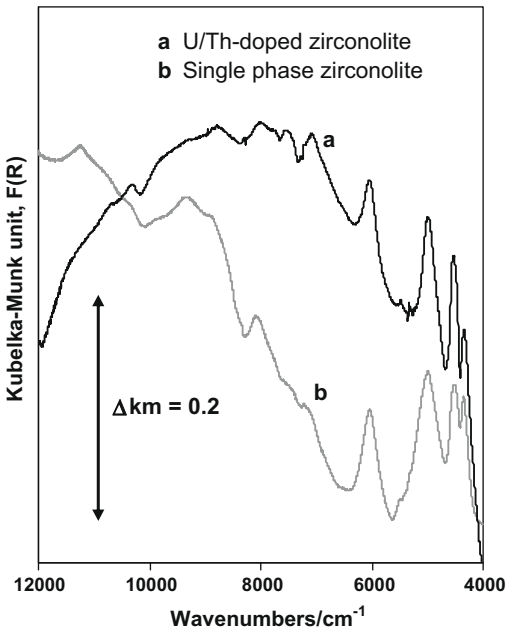


**Fig. 8.** DR spectra (4000–12,000 cm$^{-1}$) of the U/Th-doped sample and a single-phase U-doped zirconolite ($CaZr_{0.8}U_{0.2}Ti_2O_7$) sample sintered at 1250 °C in air.

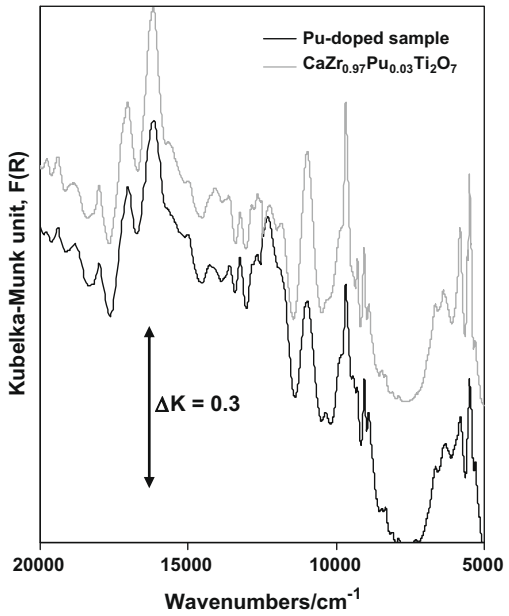


**Fig. 9.** DR spectra (5000–20,000 cm$^{-1}$) of the Pu-doped sample and a single-phase Pu-doped zirconolite ($CaZr_{0.97}Pu_{0.03}Ti_2O_7$) sintered at 1250 °C in air (spectra offset vertically to enhance visibility).

#### 3.4.2. Pu in zirconolite

Early XANES (X-ray absorption near-edge spectroscopy) studies [18–20] confirmed that tetravalent Pu ions dominate zirconolite samples sintered in air whilst ~80% $Pu^{3+}$ ions can exist in zirconolite samples sintered in a reducing atmosphere [19]. Note Pu valence states >+4 have never been found in these titanate ceramics. DR spectra (5000–20,000 cm$^{-1}$) of the bulk material together with that of a Pu-doped single-phase zirconolite

($CaZr_{0.97}Pu_{0.03}Ti_2O_7$) sintered in air are shown in Fig. 9. The similarity between these two spectra suggests that Pu presents as $Pu^{4+}$ ions in the Pu-doped sample, consistent with the previous XANES and DRS studies [18–20]. However, there is no evidence on whether the $Pu^{4+}$ has been partially reduced to $Pu^{3+}$ at the reaction interface. SEM-EDS analysis results did not provide any positive answer, noting that there would have expected stoichiometric changes if $Pu^{3+}$ formed. Nevertheless, the presence of $Pu^{3+}$ in titanate ceramics does not seem to compromise the chemical durability of the materials [21].

## 4. Conclusions

As designed, both U and Pu exist mainly as tetravalent ions in zirconolite in the waste forms for actinide immobilisation prepared by HIP using stainless steel cans for containment. The low and comparable release rates for both U/Gd and Pu/Hf pairs will decrease the criticality risk during the interim storage and long-term geological disposal of the waste form.

The waste form/HIP-can interactions under HIPing conditions do not seem to change the overall U valence, U/Pu-bearing phase distributions or produce any undesirable U/Pu-bearing phases at the reaction interface. However, whether the Pu has been reduced to trivalent at the reaction interface still remains an open question. Hence, using the criteria that the actinides remain in a stable and durable waste form phase, it can be concluded that the use of stainless steel HIP cans has no significant effect on the overall integrity of the waste form. Overall, zirconolite-based titanate ceramics are eminently suitable for immobilisation of separated actinide-rich waste streams through HIP processing technology.

## Acknowledgements

We thank T. McLeod for sample preparation, G. Smith for SEM sample preparation, K. Olufson for durability testing and P. Yee for ICP-MS analysis.

## References

[1] A.E. Ringwood, S.E. Kesson, N.G. Ware, W. Hibberson, A. Major, Nature 278 (1979) 219–223.
[2] A.E. Ringwood, S.E. Kesson, K.D. Reeve, D.M. Levins, E.J. Ramm, in: W. Lutze, R.C. Ewing (Eds.), Radioactive Waste Forms for the Future, North-Holland, Amsterdam, 1988, pp. 233–334.
[3] E.R. Vance, MRS Bull. XIX (12) (1994) 28–32.
[4] G.R. Lumpkin, Elements 2 (2006) 365–372.
[5] K.L. Smith, G.R. Lumpkin, in: J.N. Boland, J.D. Fitzgerald (Eds.), Defects and Processes in the Solid State: Geoscience Applications, The McLaren Volume, Elsevier, Amsterdam, Netherlands, 1993, pp. 401–422.
[6] K.P. Hart, G.R. Lumpkin, R. Giere, C.T. Williams, P.J. McGlinn, T.E. Payne, Radiochim. Acta 74 (1996) 309–312.
[7] V.M. Oversby, A.E. Ringwood, Radioact. Waste Manage. Nucl. Fuel Cycle 1 (1981) 289.
[8] G.R. Lumpkin, J. Nucl. Mater. 289 (2001) 136–166.
[9] M.J. Hambley, S. Dumbill, E.R. Maddrell, C.R. Scales, in: W.E. Lee, J.W. Roberts, N.C. Hyatt, R.W. Grimes (Eds.), Characterisation of 20 Year Old $^{238}$Pu-Doped Synroc C, Mater. Res. Soc. Symp. Proc., vol. 1107, 2008, pp. 373–380.
[10] R.C. Ewing, T.J. Headley, J. Nucl. Mater. 119 (1983) 102–109.
[11] G.S. Blake, G.F.H. Smith, Mineral Mag. 16 (1913) 309.
[12] S.S. Shoup, C.E. Bamberger, T.J. Haverlock, J.R. Peterson, J. Nucl. Mater. 240 (1997) 112–117.
[13] B.B. Ebbinghaus, R. Van Konynenburg, E.R. Vance, M.W. Stewart, A. Jostsons, J.S. Allender, D.T. Rankin, Ceramic Composition for Immobilization of Actinides, US Patent 6,137,025.
[14] E.R. Vance, A. Jostsons, S. Moricca, M.W.A. Stewart, R.A. Day, B.D. Begg, M.J. Hambley, K.P. Hart, B.B. Ebbinghaus, in: J.C. Marra, G.T. Chandler (Eds.), Synroc Derivatives for Excess Weapons Plutonium, Ceramics Transactions, vol. 93, American Ceramic Society, 1999, pp. 323–329.
[15] H.J. Rossell, Nature 283 (1980) 282–283.
[16] E.R. Vance, G.R. Lumpkin, M.L. Carter, D.J. Cassidy, C.J. Ball, R.A. Day, B.D. Begg, J. Am. Ceram. Soc. 85 (6) (2002) 1853–1859.
[17] Y. Zhang, E.R. Vance, K.S. Finnie, B.D. Begg, M.L. Carter, in: R. Alvarez, N.D. Bryan, I. May (Eds.), Recent Advances in Actinide Science, The Royal Society of Chemistry, 2006, pp. 343–345.
[18] X. Deschanels, V. Picot, B. Glorieux, F. Jorion, S. Peuget, D. Roudil, C. Jégou, V. Broudic, J.N. Cachia, T. Advocat, C. Den Auwer, C. Fillet, J.P. Coutures, C. Henning, A. Scheinost, J. Nucl. Mater. 352 (2006) 233–240.
[19] B.D. Begg, E.R. Vance, S.D. Conradson, J. Alloy Compd. 271–273 (1998) 221–226.
[20] E.R. Vance, K.S. Finnie, Y. Zhang, B.D. Begg, Mater. Res. Soc. Symp. Proc. 824 (2004) 249–254.
[21] B.D. Begg, Y. Zhang, E.R. Vance, S.D. Conradson, A.J. Brownscombe, Effect of Pu Valence on Acid-Dissolution of Perovskite ($CaTiO_3$), Plutonium Futures, Albuquerque, New Mexico, USA, July 6–10, 2003, Extended Abstract, Conference Proceeding, pp. 131–132.
[22] R. Dayton, H. Saller, S. Paprocki, E. Hodge, US Patent No. 687,842.
[23] M.H. Bocanegra-Bernal, J. Mater. Sci. 39 (2004) 6399–6420.
[24] H. Li, Y. Zhang, P.J. McGlinn, S. Moricca, B.D. Begg, E.R. Vance, J. Nucl. Mater. 355 (2006) 136–141.
[25] M.L. Carter, M.W.A. Stewart, E.R. Vance, B.D. Begg, S. Moricca, J. Tripp, HIPed Tailored Ceramic Waste Forms for the Immobilization of Cs, Sr and Tc, Global 2007, Boise Idaho, September 2007.
[26] M.W.A. Stewart, B.D. Begg, S. Moricca, R.A. Day, Low-Risk Tailored Waste Forms for Problematic High-level and Long-lived Nuclear Wastes, CD-ROM, 15th Pacific Basin Nuclear Conference 2006, 15–20 October 2006, Sydney, Australia.
[27] B.D. Begg, R.A. Day, S. Moricca, M.W.A. Stewart, E.R. Vance, Low-risk Waste Forms to Lock Up High-level Nuclear Waste, WM'05 Conference, February 27–March 3, 2005, Tucson, AZ, USA.
[28] M.W.A. Stewart, E.R. Vance, A. Jostsons, B.B. Ebbinghaus, J. Aust. Ceram. Soc. 39 (2) (2003) 30–48.
[29] ASTM C 1220 – 98, Standard Test Method for Static Leaching of Monolithic Wasteforms for Disposal of Radioactive Waste, ASTM International, 1998.
[30] W.W. Wendlandt, H.G. Hecht, Reflectance Spectroscopy, Wiley Interscience, New York, 1966.
[31] B.D. Begg, E.R. Vance, B.A. Hunter, J.V. Hanna, J. Mater. Res. 13 (11) (1998) 3181–3190.
[32] E.R. Vance, M.L. Carter, M.W.A. Stewart, R.A. Day, C.J. Ball, Mat. Res. Soc. Symp. Proc. 713 (2002) 319–326.
[33] M.W.A. Stewart, E.R. Vance, R.A. Day, S. Leung, A. Brownscombe, M.L. Carter, B.B. Ebbinghaus, Impurity incorporation in pyrochlore-rich ceramics, in: G.T. Chandler, X. Feng (Eds.), Ceram. Trans., vol. 107, 2000, pp. 569–576.
[34] W.T. Carnall, H.M. Crosswhite, Argonne National Laboratory Report, ANL-84-90, August 1985.